applied sciences

MDPI

*Article*

# Numerical and Experimental Investigations of Particle Dampers Attached to a Pipeline System

**Rui Ma, Fuqiang Shi, Mingxin Juan, Jiao Wang *, Jie Jin and Tao Yu ***

School of Electromechanical and Automotive Engineering, Yantai University, Yantai 264005, China; 17862817917@163.com (R.M.); 17865566300@163.com (F.S.); juanmingxin@163.com (M.J.); jinjie910@sina.com (J.J.)
* Correspondence: zoe_wjiao@163.com (J.W.); taoyuyt@126.com (T.Y.)

**Abstract:** The structure of pipeline systems is complex, and the working environment is harsh. Under the excitation of the engine equipment foundation and pump fluid, it is easy to generate excessive vibration, which seriously affects the safe operation of the equipment. Particle damping achieves structural vibration suppression through the principle of particle collision dissipation. Due to the drawbacks of traditional pipeline vibration reduction methods, this article introduces a particle damping technology for pipeline system vibration suppression and designs particle dampers based on the structural characteristics of pipelines. We analyzed the energy dissipation mechanism of particle damping, revealed the influence of the materials, structure, external excitation, and other parameters of the pipeline particle dampers on the energy dissipation characteristics of the particle damping, established a pipeline vibration reduction test system with particle damping, and verified its effectiveness in pipeline system vibration reduction. This study can provide a technical reference for vibration reduction in pipeline systems.

**Keywords:** pipeline system; particle damping; vibration suppression; energy consumption characteristics



**Citation:** Ma, R.; Shi, F.; Juan, M.; Wang, J.; Jin, J.; Yu, T. Numerical and Experimental Investigations of Particle Dampers Attached to a Pipeline System. *Appl. Sci.* **2023**, *13*, 13217. https://doi.org/10.3390/app132413217

Academic Editors: Woon-Seng Gan, Edoardo Piana, Dongyuan Shi and Jihui Aimee Zhang

Received: 13 October 2023
Revised: 27 November 2023
Accepted: 11 December 2023
Published: 13 December 2023



## 1. Introduction

Pipeline systems are generally composed of the pipeline body, joints, and support clamps, and they are connected to pumps, valves, actuators, etc. They are mainly used to transport fluid mass flow, energy flow, etc., and they are widely used in aerospace engineering, marine containers, petrochemicals, and other fields. The structure of pipeline systems is complex, and the working environment is harsh. Under the excitation of the foundation and pump source, it is easy to generate excessive vibration, leading to problems such as pipe collisions, fatigue wear, and rupture leakages in the pipeline system [1]. This seriously affects the safety of the pipeline system; therefore, there is an urgent need to adopt effective methods to suppress the vibration in pipeline systems.

The suppression of vibration in pipeline systems has always been a hot research topic. Currently, scholars have clearly attributed the vibration in pipeline systems to fluid–structure coupling vibration problems. In the area of coupled vibration problems between a constant flow and pipelines, Paidoussis [2,3] studied the instability problem of pipeline systems caused by high-speed fluid flow, the bifurcation and chaos problem of cantilever pipelines caused by steady fluid action, and the nonlinear vibration stability problem of a pipeline supported at both ends. Panda et al. [4] studied the nonlinear planar vibration of a pipeline conveying pulsating fluids caused by resonance in a two-end hinged pipeline based on harmonic variation components. Tan et al. [5] applied the nonlinear Timoshenko model to study the coupled vibration of a fluid pipeline. Tijsseling [6] revealed the coupling vibration mechanism between an unsteady fluid and pipeline system caused by the water hammer effect and proposed a fluid–structure coupling 4-, 8-, and 14-equation models. The dynamic models of pipeline systems can be classified into two types: beam models and shell models. Hu et al. [7] validated the one-dimensional control equation for pressure pulse propagation in non-viscous compressible fluids in thin-walled, naturally curved, elastic pipelines. Firouz-Abadi et al. [8] established a fluid–structure coupling dynamic model based on a shell model and derived the fluid–structure coupling field equation. The main methods for analyzing pipeline vibration include the finite element method, the characteristic line method, the transfer matrix method, etc. Ruoff et al. [9] studied the characteristics of Coriolis mass flow meters with arbitrary pipeline geometries, such as an unsteady flow, based on the finite element method. Wiggert et al. [10] predicted the response of liquid pressure and pipeline stress to the transient excitation of liquids or pipelines. Yu et al. [11] conducted theoretical research on periodic cantilever flow pipelines.

The traditional methods to reduce pipeline system vibration mainly include clamp support vibration reduction, laying viscoelastic damping materials on the surface of the pipeline, and installing tuned mass dampers on the pipeline, which have good suppression effects on the high-frequency vibrations of the pipeline. The shortcomings are the limited installation position as well as the easy deformation, aging, and failure of the damping materials, which can only achieve a vibration reduction of a single frequency band. Wang et al. [12] demonstrated that clamp fixtures have a good inhibitory effect on the vibration of pipeline systems. Zi et al. [13] proposed using long, coated damping structures made of metal wire materials for vibration reduction in the high-temperature pipelines on ships. Jiang et al. [14] verified the vibration reduction effect of a tuned mass damper in an underwater pipeline system through experiments.

Particle damping achieves energy dissipation through collisions and friction between particles and between particles and the container wall. This technology has the advantages of a wide temperature range, wide frequency domain, radiation resistance, and high reliability [15–17]. Masri et al. [18] derived an analytical solution for a particle impact damper under sinusoidal excitation. Xu et al. [19] proposed considering the influence of shear friction on damping performance based on an elastic beam and plate structure with embedded particle collision dampers. Jin et al. [20] designed an aircraft pipeline particle damper and analyzed the energy dissipation mechanism of the damper and the influence of different parameters on the damping energy dissipation. Meyer et al. [21] combined the discrete element model with a simplified finite element model and proposed a contact algorithm for predicting system motion. Jin et al. [22] used the least squares method and the Prony method to predict the damping coefficient of a tuned particle impact damper. Yang et al. [23] studied the influence of parameters such as filling particle size on the damping and mass characteristics of dampers through experiments based on power measurement technology. Romdhane et al. [24] proposed an experimental characterization method for the loss factor of non-blocking particle dampers using system parameters such as excitation amplitude under harmonic excitation. Wang et al. [25] designed a particle damper for pipeline systems and analyzed the influence of parameters such as the material, structure, boundary conditions, etc., on damping performance under harmonic excitation. Guo et al. [26] revealed the influence of particle size and quantity in the low-frequency range on the energy dissipation characteristics of particle dampers. Ż Urawski et al. [27] analyzed the vibration and energy dissipation characteristics of a cantilever beam-tuned particle damper with different particle masses and container volumes.

Many scholars have conducted extensive research on the mechanism of particle damping energy dissipation; however, there are relatively few studies on vibration reduction in pipeline systems. Therefore, this article introduces a particle damping technology for pipeline systems. Through a theoretical analysis and simulation, the influence of damper parameters on particle damping characteristics was revealed. At the same time, combined with experimental testing, it was verified that the particle dampers have good vibration reduction performance. This research provides a technical reference for the development of vibration suppression approaches for pipeline systems.

## 2. The Theory of Particle Damping Energy Dissipation

Particle damping achieves energy dissipation through collision and friction between particles, as well as between the particles and the container wall.

### 2.1. Analysis of Normal Particle–Particle Collisions

The normal particle collision deformation diagram and contact model are shown in Figures 1 and 2, respectively. In these figures, $r_a$, $R$, $F_n$, $\delta_n$, $k_n$, $c_n$, and $m$ are the contact surface radius, the particle radius, normal force, relative displacement, normal stiffness, normal damping coefficient, and particle mass, respectively.

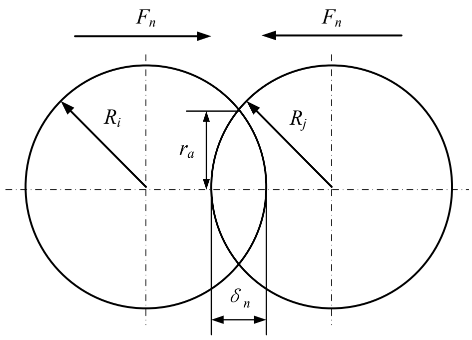


**Figure 1.** Schematic diagram of normal collision deformation of particles.

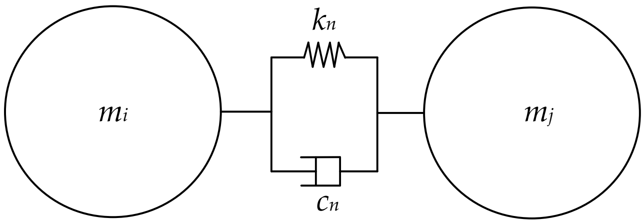


**Figure 2.** Particle normal collision contact model.

The normal overlap after contact deformation between particles is expressed as

$$\delta_n = R_i + R_j - \left|c_i - c_j\right| > 0 \tag{1}$$

where $c_i$ and $c_j$ are the displacement vectors of the particle centers.

The normal stiffness is expressed as

$$k_n = 2E^* \sqrt{R^* \delta_n} \tag{2}$$

where $E^*$ and $R^*$ are the effective elastic modulus and effective radius of the particle, respectively. They can be expressed as

$$\begin{cases} \frac{1}{E^*} = \frac{1-\mu_i^2}{E_i} + \frac{1-\mu_j^2}{E_j} \\ R^* = \frac{1}{R_i} + \frac{1}{R_j} \end{cases} \tag{3}$$

The normal damping coefficient $c_n$ is expressed as

$$c_n = 2\sqrt{\frac{5}{6}}\gamma\sqrt{k_n m^*} \tag{4}$$

where $m^*$ is the effective mass of the particle, and $\gamma$ is the critical damping coefficient. $m^*$ and $\gamma$ are expressed as

$$\begin{cases} m^* = \frac{m_i m_j}{m_i + m_j} \\ \gamma = \frac{\ln e}{\sqrt{\ln^2 e + \pi^2}} \end{cases} \tag{5}$$

where $e$ is the coefficient of restitution of the particle.

### 2.2. Analysis of Tangential Particle–Particle Collisions

The particle tangential collision contact model is shown in Figure 3, where $k_t$, $c_t$, and $\mu_f$ are the tangential stiffness, tangential damping coefficient, and the friction coefficient, respectively.

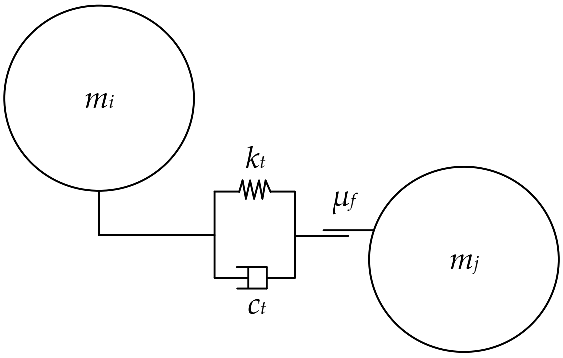


**Figure 3.** Particle tangential collision contact model.

The tangential stiffness $k_t$ is expressed as

$$k_t = 8G^* \sqrt{R^* \delta_n} \tag{6}$$

where $G^*$ is the effective shear modulus, which is expressed as

$$\frac{1}{G^*} = \frac{1-\mu_i}{G_i} + \frac{1-\mu_j}{G_j} \tag{7}$$

where $G_i$ and $G_j$ are the shear moduli of the particles, and $\mu_i$ and $\mu_j$ are the static friction coefficients for particle contact.

The tangential damping coefficient $c_t$ is expressed as

$$c_t = 2\sqrt{\frac{5}{6}}\gamma\sqrt{k_t m^*} \tag{8}$$

where $m^*$ and $\gamma$ can be calculated from Equation (5).

### 2.3. Analysis of Contact Mechanism between a Particle and the Container Wall

Figure 4 shows the normal and tangential contacts between a particle and the container wall. In Figure 4, $F_n$ and $F_t$ are the normal and tangential forces of the particle on the container wall, respectively; $F_n{}'$ and $F_t{}'$ are the reaction forces of the container wall on the particle, $k_{cn}$ and $k_{ct}$ are the normal and tangential stiffnesses between the particle and container wall, respectively; and $c_{cn}$ and $c_{ct}$ are the normal and tangential damping coefficients between the particle and the container wall, respectively.

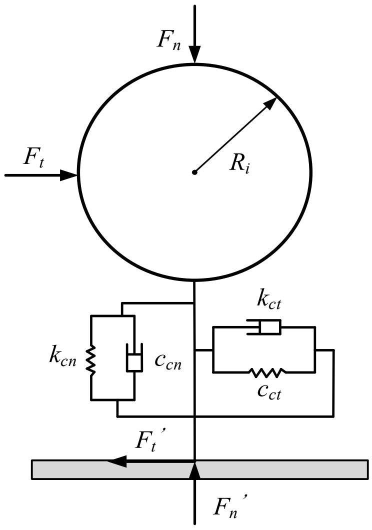


**Figure 4.** Schematic diagram of contact between a particle and the container wall.

#### 2.3.1. Normal Contact between a Particle and the Container Wall

The force between a particle and the container wall in the normal direction is expressed as

$$F_n{}' = k_{cn}\delta_c + 2\zeta\sqrt{m_i k_{cn}}\dot{\delta}_c \tag{9}$$

where $m_i$ is the mass of the particle, $\delta_c = R_i - l_i$ is the normal relative displacement between the particle and the container wall, and $\dot{\delta}_c$ is the velocity between the particle and the container wall.

The normal stiffness between the particle and the container wall is expressed as

$$k_{cn} = \frac{4\sqrt{R_i}}{3}\left(\frac{1-\mu_i^2}{E_i} + \frac{1-\mu_c^2}{E_c}\right)^{-1} \tag{10}$$

where $E_i$ and $E_c$ and $\mu_i$ and $\mu_c$ are the elastic moduli and the Poisson's ratios of the particle and container wall, respectively.

The normal damping coefficient between the particle and the container wall is expressed as

$$c_{cn} = 2\sqrt{\overline{m}k_{cn}} \tag{11}$$

where $\overline{m}$ is the mass of the particle.

#### 2.3.2. Tangential Contact between a Particle and the Container Wall

The force between the particle and the container wall in the tangential direction is expressed as

$$F_t{}' = \frac{-\mu_s F_n{}'\dot{\delta}_s}{\left|\dot{\delta}_s\right|} \tag{12}$$

where $\mu_s$ is the coefficient of friction between the particle and the container wall, and $\dot{\delta}_s$ is the tangential velocity of the particle with respect to the container wall.

The tangential stiffness between the particle and the container wall is expressed as

$$k_{ct} = \alpha k_{cn} \tag{13}$$

where $\alpha$ is the scaling factor.

The tangential damping coefficient between the particle and the container wall is expressed as

$$c_{ct} = 2\sqrt{\overline{m}k_{ct}} \tag{14}$$

*2.4. Analysis of Particle Damping Energy Dissipation Mechanism*

Assuming that no sliding occurs between particles, the collision energy dissipation in the normal and tangent directions is expressed as

$$\begin{cases} \Delta E_n = \frac{1}{2}\frac{m_i m_j}{m_i+m_j}\left(1-e_n^2\right)\left|v_{rn}^-\right|^2 \\ \Delta E_t = \frac{1}{2}\frac{m_i m_j}{m_i+m_j}\left(1-e_t^2\right)\left|v_{rt}^-\right|^2 \end{cases} \tag{15}$$

where $e_n$ and $e_t$ are the normal and tangential recovery coefficients between particles, which are expressed as

$$\begin{cases} e_n = \frac{v_{jn}^+ - v_{in}^+}{v_{in}^- - v_{jn}^-} = \frac{v_{rn}^+}{v_{rn}^-} \\ e_t = \frac{v_{jt}^+ - v_{it}^+}{v_{it}^- - v_{jt}^-} = \frac{v_{rt}^+}{v_{rt}^-} \end{cases} \tag{16}$$

where $v_{in}$ and $v_{jn}$ and $v_{it}$ and $v_{jt}$ are the normal and tangential velocities of the particles, with the superscripts '−' and '+' representing the conditions before and after the collisions, respectively.

When the tangential force between particles is greater than the maximum static friction force, friction energy dissipation will replace tangential collision energy dissipation. The friction energy dissipation is expressed as

$$\Delta E_f = \mu_f |F_n \delta_t| \tag{17}$$

where $\mu_f$ and $\delta_t$ are the friction coefficient and the tangential relative displacement between particles, respectively. $F_n$ is the normal force between particles, the expression of which is obtained from the Hertz contact theory [28]:

$$F_n = \frac{4}{3}E^*\sqrt{R^*}\delta_n^{\frac{3}{2}} \tag{18}$$

Due to the small contact area between the particle and the container wall, the analysis method for energy dissipation is also applicable to the energy dissipation between the particle and the container wall. Therefore, the energy dissipation for the particle damping system is expressed as

$$E = \Sigma\Delta E_n + \Sigma\Delta E_t + \Sigma\Delta E_f \tag{19}$$

where $\sum\Delta E_n$, $\sum\Delta E_t$, and $\sum\Delta E_f$ represent the total normal and tangential collision energy consumption, and friction energy consumption of the particle collision damping system, respectively.

## 3. Design and Simulation of Particle Damper

*3.1. Design of the Particle Damper*

A pipeline with an outer diameter of 0.016 m was selected, and a particle damper was designed for the pipeline system based on the structural characteristics of the pipeline. A damper design should meet the following requirements: (1) it can accommodate enough particles; (2) it has good structural sealing; (3) it is lightweight; and (4) it is easy to install and disassemble. Two materials and three cavity structures were used to fabricate pipeline particle dampers, and their structural diagrams and shape parameters are shown in Tables 1 and 2, respectively.

**Table 1.** Structural diagram of pipeline particle collision damper.

| | Two Cavities | Four Cavities | Six Cavities |
|---|---|---|---|
| Design drawing |  | 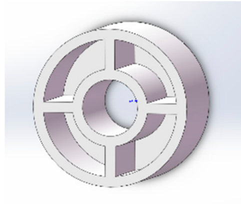 | 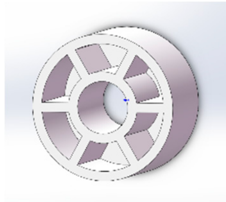 |
| ABS | 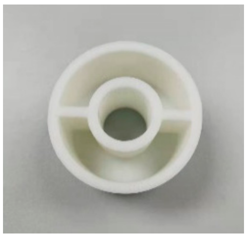 | 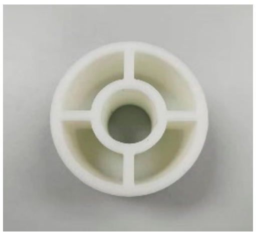 | 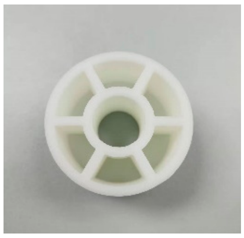 |
| Aluminum alloy |  |  |  |

**Table 2.** Structural parameters of the particle damper.

| Inner Diameter | Outer Diameter | Container Height | Wall Plate Thickness | Cover Plate Thickness |
|---|---|---|---|---|
| 16.5 mm | 46 mm | 28 mm | 3 mm | 1 mm |

*3.2. Modeling of Particle Damper Using EDEM*

The modeling of the particle damper in the discrete element software EDEM 2020 is shown in Figure 5.

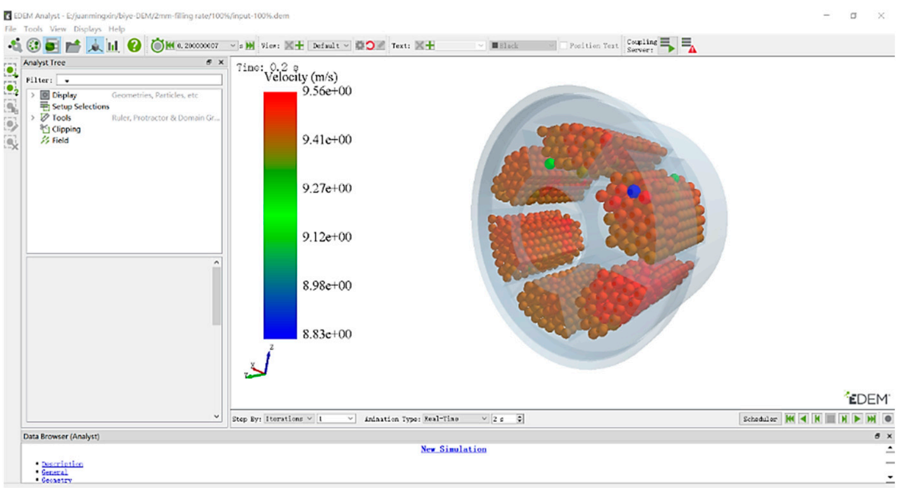


**Figure 5.** Modeling of particle damper.

The simulation process of the EDEM software is mainly divided into three parts: modeling, dynamic simulation, analysis, and post-processing.

### 3.3. Simulation Parameter Settings

The discrete cavity software EDEM was used to simulate the state of motion and energy consumption of the particle system. The contact type was set to Hertz–Mindlin (no slip), and the materials and contact parameters used in the simulation are shown in Tables 3 and 4, respectively. According to the actual working conditions, the simulation selected the time step to be 25% of the Rayleigh time step, and the grid size was 2.5 times the minimum radius of the filled particle.

**Table 3.** Material parameters.

| Material | Density (ρ) (kg·m$^{-3}$) | Elasticity Modulus (E) (GPa) | Poisson Ratio (μ) |
|---|---|---|---|
| Steel | 7850 | 200 | 0.3 |
| Aluminum alloy | 2800 | 68.9 | 0.33 |

**Table 4.** Contact parameters.

| Contact | Coefficient of Recovery | Coefficient of Static Friction | Coefficient of Rolling Friction |
|---|---|---|---|
| Steel–Steel | 0.45 | 0.15 | 0.15 |
| Steel–Aluminum alloy | 0.45 | 0.17 | 0.001 |

### 3.4. Analysis of the Influence of Particle Damper Materials and Structural Parameters

#### 3.4.1. Particle Filling Rate

The particle damper was filled with 2 mm steel particles; the other conditions remained the same. The number of particles and the corresponding mass ratios at different filling rates are shown in Table 5.

**Table 5.** Number of particles and mass ratios corresponding to different filling rate.

| Filling Rate (%) | Number of Particles | Mass Ratio (%) |
|---|---|---|
| 10 | 203 | 6.68 |
| 20 | 406 | 13.35 |
| 30 | 609 | 20.03 |
| 40 | 812 | 26.73 |
| 50 | 1015 | 33.38 |
| 60 | 1218 | 40.05 |
| 70 | 1421 | 46.73 |
| 80 | 1624 | 53.40 |
| 90 | 1827 | 60.08 |
| 100 | 2030 | 66.75 |

From Figure 6, it can be seen that the total energy dissipation of the particle system shows a trend of increasing and then decreasing with an increase in the particle filling rate. The total energy dissipated by the particle system was highest at the 60% filling rate. There was an optimal particle filling rate for particle dampers in such conditions. When the particle filling rate was low, the number of particles in the container was low, the particle–particle and particle–container wall contact was limited, and less energy was dissipated through collisions and friction. As the particle filling rate increased, the momentum exchange between particles and between particles and the container wall increased, and the total energy dissipated by the particle system increased. When the filling rate of the particles was higher than the optimal filling rate, the space for movement of the particles inside the container wall was limited, and the energy dissipated through collisions and friction decreased gradually. At a 100% filling rate, the particles had very little movement, but energy could still be dissipated through friction between the particles. Therefore, the total energy dissipated at this filling rate was slightly better than that at a 10% filling rate.

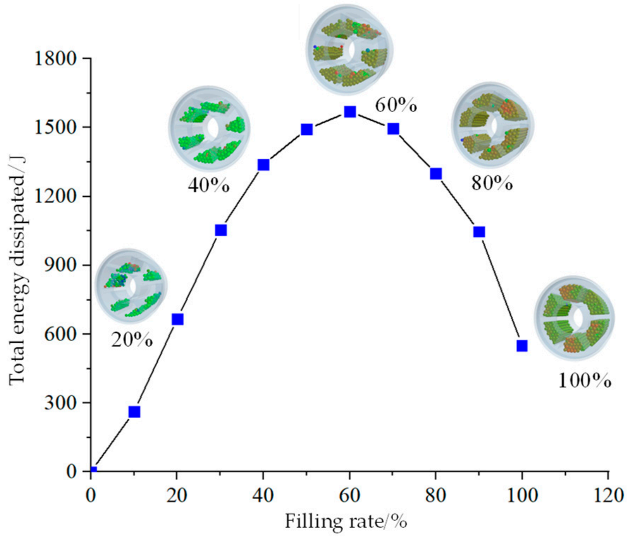


**Figure 6.** Total energy dissipated by the system with different particle filling rate.

### 3.4.2. Particle Size

Particle size is one of the most important parameters for the energy dissipated by a damper. With all the other parameters being equal, the steel particles with particle sizes of 1 mm, 1.5 mm, 2 mm, 2.5 mm, 3 mm, 3.5 mm, and 4 mm were tested at three filling rates of 20%, 60%, and 80%. The filling effect of the different particle sizes in the damper is shown in Figure 7.

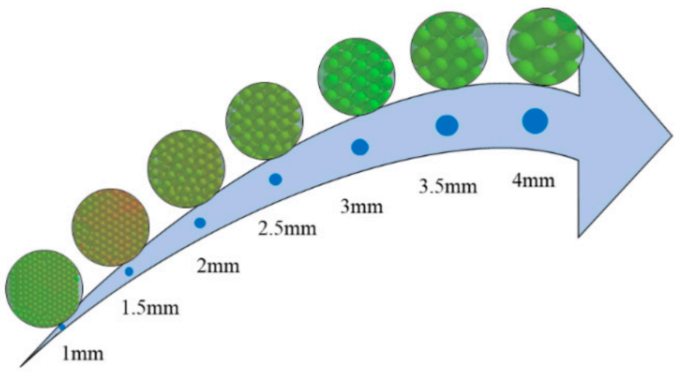


**Figure 7.** Filling effect of different particle sizes in the damper.

As shown in Figures 8 and 9, at the same particle filling rate, the total energy dissipated by the particle system decreased as the particle size increased. Due to the spatial environment in which the particles were located, the larger the particle size, the fewer particles there were in the damper cavity. This resulted in fewer particle collisions and, therefore, less total energy dissipation in the particle system. At the three particle filling rates, it was observed that the total energy dissipated in the particle system was greatest at the 60% filling rate, followed by the 80% filling rate, and the least dissipation at the 20% filling rate.

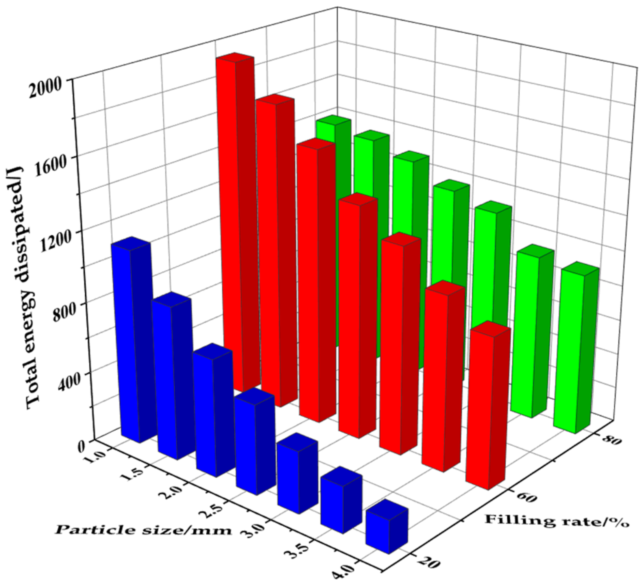


**Figure 8.** Total energy dissipated by particle system with the same particle size.

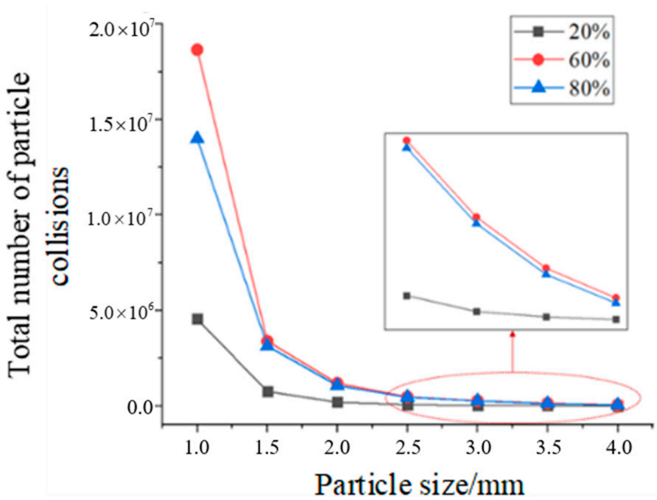


**Figure 9.** Total number of particle collisions for different particle sizes.

3.4.3. Particle Density

Particle density was an important parameter in the simulation. The influence of different particle densities (2000, 5000, 7850, 11,000, and 14,000 kg/m$^3$) on the total energy dissipation of the particle system was investigated at three filling rates (20%, 60%, and 80%).

As shown in Figure 10, the total energy dissipation of the particle damper system increased with particle density at all three filling rates. When the particle size is the same, the mass of the particles with a lower density is much smaller. Under vibration conditions, the motion of the particle system was relatively low, and the contact with the damper system as a whole was relatively small. Therefore, the overall energy consumption of the particle system was low. Meanwhile, denser particles have a relatively large mass, and the particle system makes more contacts. The collisions and friction between particles and between particles and the container walls were more prominent. Therefore, a larger energy dissipation was achieved.

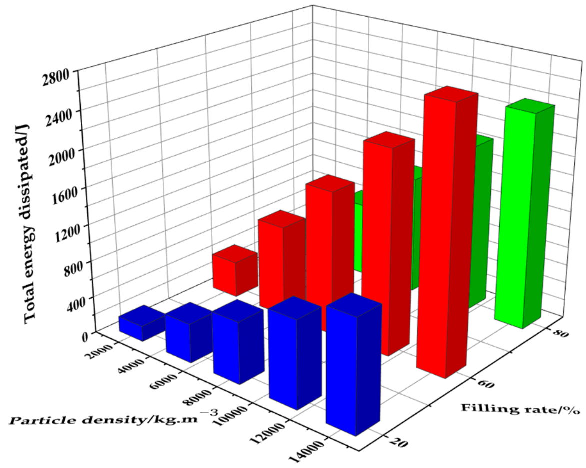


**Figure 10.** Total energy dissipated by the system for different particle densities.

#### 3.4.4. Particle Recovery Coefficient

The particle recovery coefficient characterizes the energy dissipation effect due to the normal relative motion that occurs during collisions between particles and between particles and the container walls. It is an important index for studying the energy dissipation characteristics of a particle system. The effects of different particle recovery coefficients (0.15, 0.3, 0.45, 0.6, and 0.75) on the total energy dissipation of the particle system and the total normal energy dissipation at three filling rates were obtained (Figures 11 and 12).

As shown in Figures 11 and 12, as the particle recovery coefficient increased, both the total energy dissipated and the normal total energy dissipated by the particle system showed a gradual decreasing trend. The smaller the particle recovery coefficient was, the stronger the particle recovery ability was, and the greater the mechanical energy dissipated, the greater the overall dissipated energy of the particle system was. When the particle recovery coefficients were the same but the filling rate was different, a smaller filling rate of the particles resulted in a smaller proportion of space occupied by the particles in the damper cavity. The normal relative velocity of the particles decreased as a result of the increase in motion travel. The number of effective contacts between particles and between particles and the container walls decreased, and the contact collision dissipation of total energy decreased. When the particle filling rate is at a more favorable value, the total energy supplied by the damper to the particle system achieves greater dissipation through the contact body system.

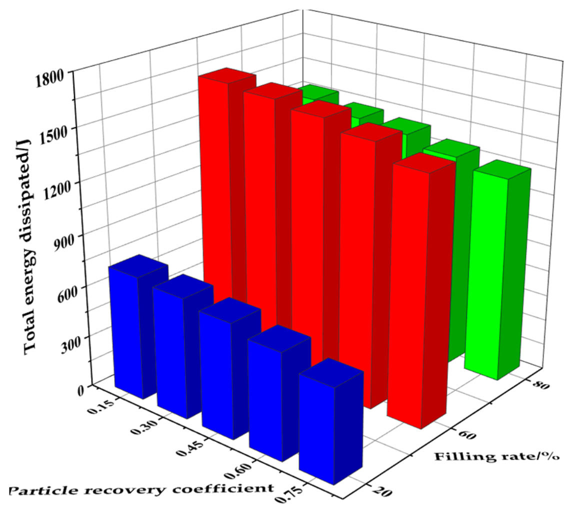


**Figure 11.** Total energy dissipated with different particle recovery coefficients.

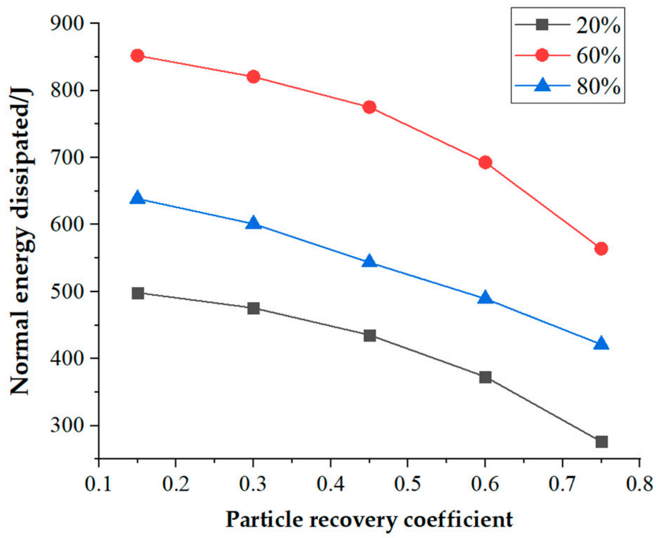


**Figure 12.** Normal energy dissipated with different particle recovery coefficients.

### 3.4.5. Contact Body Friction

The friction coefficient is another important parameter affecting the total energy dissipated by the pellet system. The friction coefficients between particles and particles were set at 0.15, 0.35, 0.55, 0.75, and 0.95, and the friction coefficients between particles and the container wall were set at 0.17, 0.37, 0.57, 0.77, and 0.97. The influence of these friction coefficients between different contact bodies on the total energy dissipated by the particle system is shown in Figure 13.

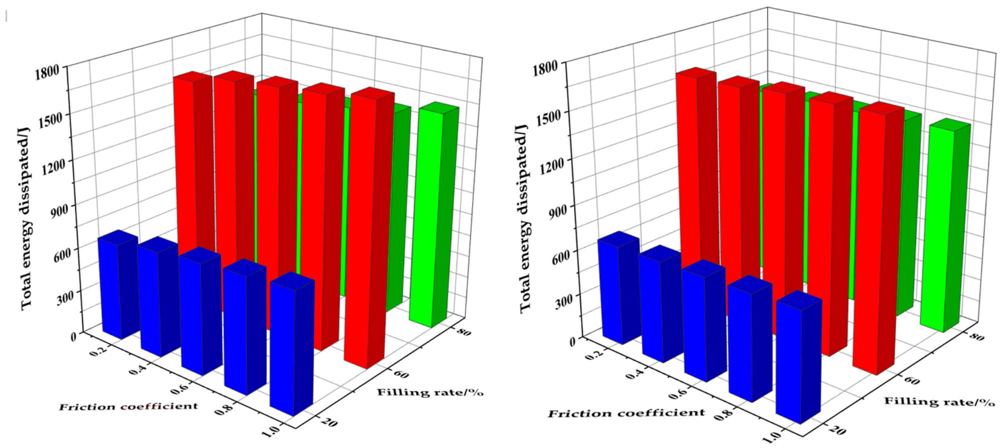


(**a**) Between particles. (**b**) Between particles and container walls.

**Figure 13.** Total energy dissipated with different friction coefficients between contact bodies.

As shown in Figure 13, the total energy dissipated by the particle system tended to increase as the friction coefficients between particles and between particles and the container walls increased. Since the total energy dissipated by the particle system includes collision energy dissipated and friction energy dissipated, under the same working conditions, a larger friction coefficient between particles resulted in a larger friction energy dissipated by friction. The total energy dissipated by the particle system also increased.

3.4.6. Damper Structure

The energy dissipation characteristics of particle dampers also change depending on the damper structure. Particle collision dampers with two-, four-, and six-cavity damper cavity structures were tested. Their effects on the total energy dissipation of the particle system were investigated at three filling rates of 20%, 60%, and 80%.

As shown in Figure 14, the total energy dissipated by the particle system increased and then decreased with the number of damper cavities when the particle filling rate was the same. When the damper was a two-cavity structure, the space in a single cavity of the particle damper was larger, allowing for higher free motion travel of the particles in the cavity. Therefore, the effective contact energy dissipation between particles and between particles and the container wall was reduced. As the number of damper cavities increased, the space in the individual cavities of the damper became smaller, the traveling distance of the particle system became shorter, and the energy dissipated due to collisions and friction increased. When the space in the individual cavities of a particle damper was small, the motion of the particles inside the container was limited. The ability to dissipate energy through collisions and friction between contacting bodies was reduced, and thus the total energy dissipated was reduced.

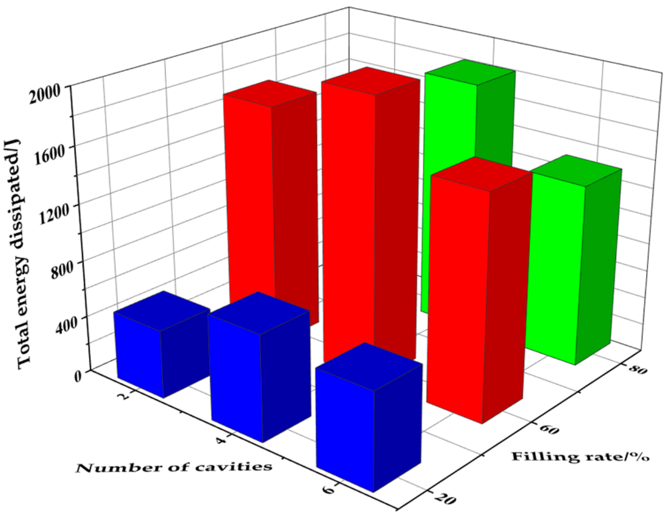


**Figure 14.** Total energy dissipated with different numbers of damper cavities.

*3.5. Analysis of the Effect of External Excitation Parameters of a Particle Damper*

3.5.1. Excitation Frequency

A particle damper is capable of energy dissipation in a wide frequency domain. A sinusoidal excitation was applied in the x-direction of the damper. The excitation frequencies of 50, 300, 600, 900, 1200, 1500, 1800, and 2000 Hz were tested.

Figure 15 shows that the total energy dissipated by the system increased with the increase in the excitation frequency. The total energy dissipated by the particle system at higher excitation frequencies increased much more than at lower excitation frequencies. The higher the excitation frequency, the greater the number of vibrations per cavity of time for a particle damper. The number of particle–particle and particle–container wall interactions increased, and the total energy dissipated through collisions and friction increased. At the same time, at different filling rates, the number of particles also affected the total energy dissipated by the particle system.

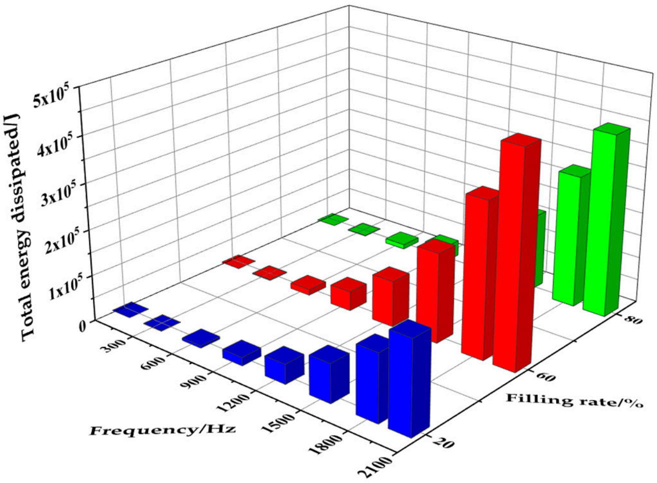


**Figure 15.** Total energy dissipated at different excitation frequencies.

3.5.2. Amplitude Displacement

In order to investigate the effect of the displacement amplitude of the particle damper on the total energy dissipation of the particle system, different displacement amplitudes (2 mm, 4 mm, 6 mm, 8 mm, and 10 mm) were applied to the damper in the x-direction.

As shown in Figure 16, as the displacement amplitude of the damper structure increased, the total energy dissipated by the particle system became larger and larger. This was due to the fact that the displacement amplitude of the damper structure changed the motion of the particles inside the container. The intensity of the motion of the particles in the damper cavity increased with the amplitude of the displacement of the structure. The momentum exchange between the particles and the damper system increased, and the total energy dissipated by the particle system increased. For the same displacement amplitude, the total energy dissipated by the particle system increased with the filling rate. The maximum value of the total energy dissipated by the particle system was found at an amplitude displacement of 10 mm and a particle filling rate of 60%.

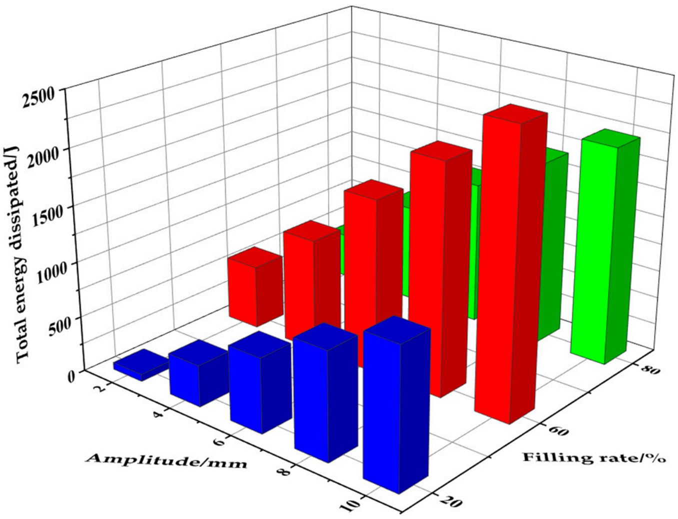


**Figure 16.** Total energy dissipated for different displacement amplitudes.

## 4. Experimental Verification of the Damping Performance of the Pipeline System

### *4.1. Test System Set-Up*

A testing platform to measure the vibration characteristics of a particle damper pipeline was established. A basic harmonic excitation test was conducted on the cantilever pipeline with and without particle dampers. The LMS vibration testing and analysis system was used to collect vibration signals from the pipeline. During the test, the vibration table is loaded along the X direction (horizontal and vertical to the pipeline). According to the vibration mode of the cantilever pipeline (with a length of 0.5 m, an outer diameter of 0.016 m, and a wall thickness of 0.001 m), a lightweight acceleration sensor (PCB, model 352C22) was attached to the pipeline. The measurement point was 1/3 of the pipeline length away from the free end, and the particle damper was located at the free end of the pipeline. The experimental instrument and vibration table (ES-10-240, frequency range 2–5000 Hz) layout are shown in Figure 17.

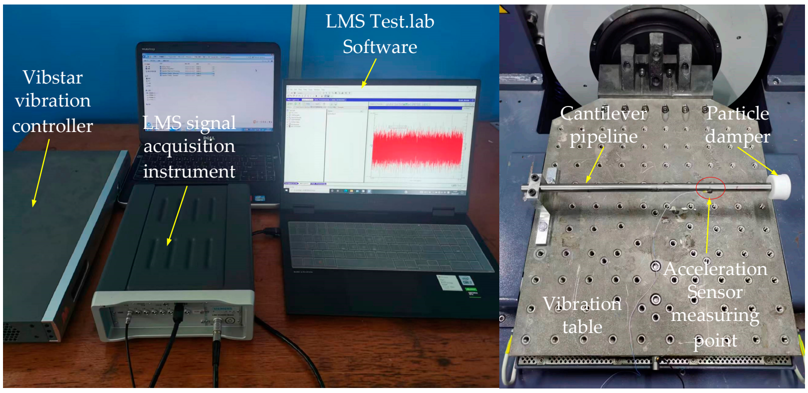


**Figure 17.** Experimental setup for the vibration test.

### *4.2. Damping Performance Test of Particle Damper under Basic Harmonic Excitation*

#### 4.2.1. Influence of Different Materials of Four-Cavity Dampers on the Vibration Damping Performance of Pipeline

The four-cavity particle dampers made of two materials that were used in the test are shown in Figure 18. The dampers were filled with steel particles with a particle size of 2 mm using a 60% filling rate.

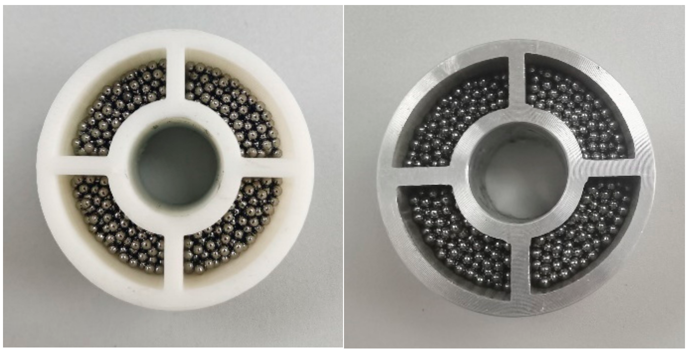

(**a**) ABS. (**b**) Aluminum alloy.

**Figure 18.** Filling effect of four-cavity particle damper made of two different materials.

The frequency range of the sinusoidal swept excitation was 10–2000 Hz, and the resonance frequencies of the bare pipeline and the four-cavity particle damper with different materials were obtained. The first-order resonance frequency was chosen to be the sinusoidal frequency, and the excitation frequencies tested were 83 Hz, 46 Hz, and 43 Hz, and the comparative time and frequency domain responses of the pipeline system before and after the addition of the four-cavity particle damper with different materials were obtained (Figure 19).

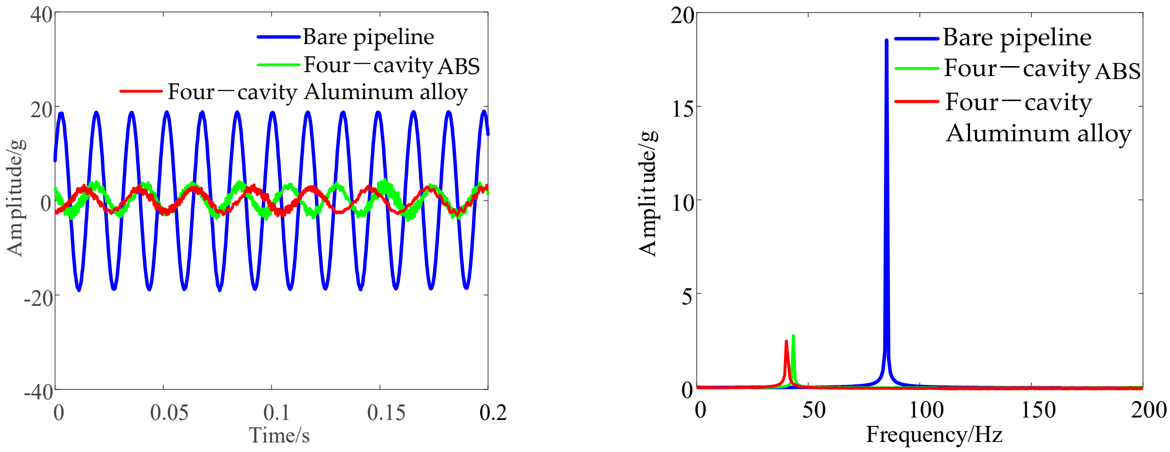


(**a**) Time domain response. (**b**) Frequency domain response.

**Figure 19.** Vibration response of a four-cavity particle damper using two different materials.

As shown in Figure 19, the time domain and frequency domain responses of the tubing with the particle damper made of two different materials were significantly reduced compared to that of the bare pipeline. The first-order frequency of the four-cavity particle dampers made of ABS and aluminum alloy was reduced by 83.66% and 85.29%, respectively, compared to that of the bare pipeline. The first-order amplitude of the four-cavity particle damper made of aluminum alloy decreased by about 9.97% compared with that of the damper made with ABS. This shows that the particle damper with these two materials can achieve good damping effects, and the four-cavity damper made of aluminum alloy has better damping effects.

#### 4.2.2. Influence of Different Materials of Six-Cavity Dampers on the Vibration Damping Performance of Pipeline

Six-cavity particle dampers made of ABS or aluminum alloy were tested and are shown in Figure 20. The damper was filled with steel particles with a particle size of 2 mm and a filling rate of 60%.

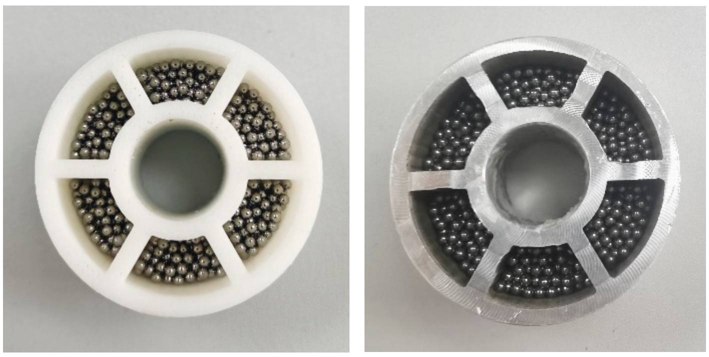

(**a**) ABS. (**b**) Aluminum alloy.

**Figure 20.** Filling effect of six-cavity particle dampers made of two materials.

The ABS and aluminum alloy six-cavity particle dampers were attached to the cantilever pipeline. The excitation frequencies used were 83 Hz, 49 Hz, and 45 Hz, and the comparative time and frequency domain responses of the pipeline system before and after the attachment of the six-cavity particle damper made of different materials are shown in Figure 21.

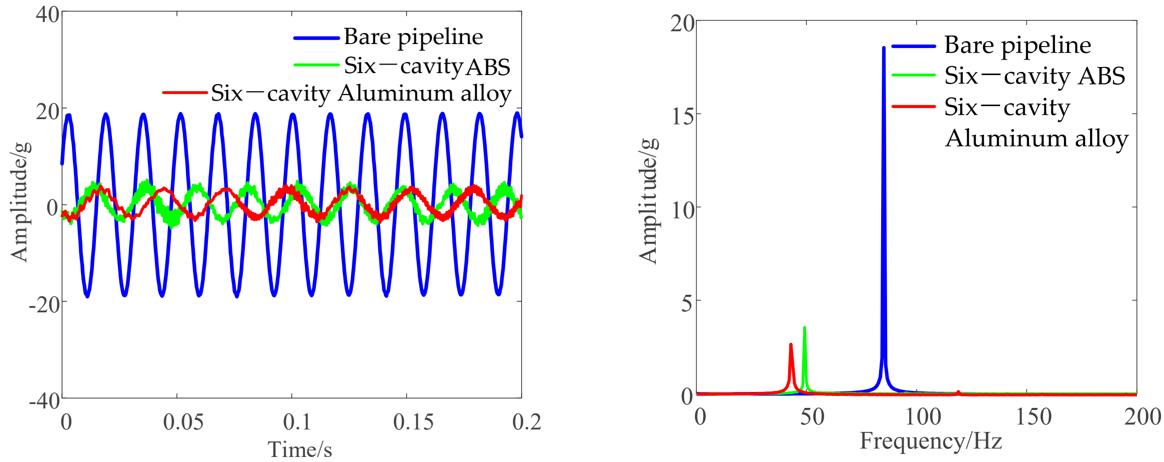


(**a**) Time domain response. (**b**) Frequency domain response.

**Figure 21.** Vibration response of a six-cavity particle damper made of two different materials.

As shown in Figure 21, compared with the bare pipeline, the time and frequency domain responses of the six-cavity particle dampers attached to the pipeline were greatly reduced. The frequency domain amplitudes corresponding to the first-order frequency were reduced by 80.35% and 84.20%, respectively. The frequency domain amplitude of the six-cavity particle damper with aluminum alloy material added to the pipeline was the smallest at about 2.91 g. Meanwhile, compared to the ABS material six-cavity particle damper, the frequency domain amplitude decreased by about 19.61%. This indicates that the six-cavity damper made of aluminum alloy had a better damping effect.

## 5. Conclusions

Particle damping technology was introduced into a pipeline system. The energy dissipation mechanism of particle damping was analyzed via numerical calculations and experimental testing. The particle damper for pipeline systems was designed, and the effects of the damper material and structure, external excitation, and other parameters on the energy dissipation characteristics of particle damping were revealed. The vibration suppression test of the designed particle damper in a pipeline system was performed. The main conclusions of this paper are as follows:

1. The total energy dissipated in the particle system shows a trend of increasing and then decreasing with an increasing filling rate. The highest total energy dissipated by the particle system was achieved when the filling rate was 60%. When the damper space is a constant value, the number of particles and energy dissipated in the particle system decreases with increasing particle size. The total energy dissipated by the particle system increases with increasing particle density.
2. The total energy dissipated by the particle system increases with increasing particle density, increasing particle–particle and particle–container wall friction coefficients, and decreasing recovery coefficients. The total energy dissipated in the particle system shows a tendency to increase and then decrease with increasing numbers of damper cavities, and the highest total energy dissipated in the particle system was achieved with a four-cavity structure.
3. The total energy dissipated by the particle system increases with increasing excitation frequency, amplitude displacement, and number of the damper structure. The frequency domain amplitude of the aluminum alloy damper pipeline decreased by 9.97% and 19.61% for the four-cavity and six-cavity damper configurations, respectively, compared with that of the ABS. This indicates that the damping effect of aluminum alloy particle damper cavities is better than that of ABS dampers.
4. For both ABS and aluminum alloy damper structures, the frequency domain amplitudes of the four-cavity damper were smaller than that of the six-cavity ones. This

indicates that four-cavity particle dampers have a better damping effect on pipeline systems. Under basic harmonic excitation, the damping effects of the two materials and two-cavity structures have the same pattern when attached to the pipeline.

**Author Contributions:** Methodology, R.M. and F.S., Software, T.Y., Validation, J.W., Formal analysis, J.J., Investigation, R.M., Data curation, F.S., Writing—original draft, R.M., Writing—review and editing, J.J., Project administration, M.J. All authors have read and agreed to the published version of the manuscript.

**Funding:** This research was funded by Provincial Natural Science Foundation of China, grant number ZR2020ME121.

**Institutional Review Board Statement:** Not applicable.

**Informed Consent Statement:** Not applicable.

**Data Availability Statement:** The data used to support the findings of this study are available from the corresponding author upon request. The data are not publicly available due to privacy.

**Conflicts of Interest:** The authors declare no conflict of interest.

## References

1. Gao, P.; Yu, T.; Zhang, Y.; Wang, J.; Zhai, J. Vibration analysis and control technologies of hydraulic pipeline system in aircraft: A review. *Chin. J. Aeronaut.* **2021**, *34*, 83–114. [CrossRef]
2. Paidoussis, M.P. *Fluid-Structure Interactions: Slender Structures and Axial Flow*; Academic Press: Cambridge, MA, USA, 1998.
3. Paidoussis, M.P.; Li, G.X. Pipes conveying fluid: A model dynamical problem. *J. Fluids Struct.* **1993**, *7*, 137–204. [CrossRef]
4. Pan Da, L.N.; Kar, R.C. Nonlinear dynamics of a pipe conveying pulsating fluid with parametric and internal resonances. *Nonlinear Dyn.* **2007**, *49*, 9–30. [CrossRef]
5. Tan, X.; Ding, H.; Chen, L.Q. Nonlinear frequencies and forced responses of pipes conveying fluid via a coupled Timoshenko model. *J. Sound Vib.* **2019**, *455*, 241–255. [CrossRef]
6. Tijsseling, A.S. Fluid-structure interaction in liquid-filled pipe systems: A review. *J. Fluids Struct.* **1996**, *10*, 109–146. [CrossRef]
7. Hu, C.K.; Phillips, J.W. Pulse propagation in fluid-filled elastic curved tubes. *J. Press. Contain. Technol. Trans. ASME* **1981**, *103*, 43–49. [CrossRef]
8. Firouz-Abadi, R.D.; Noorian, M.A.; Haddadpour, H. A fluid–structure interaction model for stability analysis of shells conveying fluid. *J. Fluids Struct.* **2010**, *26*, 747–763. [CrossRef]
9. Ruoff, J.; Hodapp, M.; Kück, H. Finite element modelling of coriolis mass flowmeters with arbitrary pipe geometry and unsteady flow conditions. *Flow Meas. Instrum.* **2014**, *37*, 119–126. [CrossRef]
10. Wiggert, D.C.; Hatfield, F.J.; Stuckenbruck, S. Analysis of liquid and structural transients in piping by the method of characteristics. *J. Fluids Eng.* **1987**, *109*, 161–165. [CrossRef]
11. Yu, D.; Païdoussis, M.P.; Shen, H.; Wang, L. Dynamic stability of periodic pipes conveying fluid. *J. Appl. Mech.* **2014**, *81*, 011008. [CrossRef]
12. Wang, J.; Chen, G.; Zheng, Q.H. Effect of clamp on aircraft hydraulic pipeline dynamic stress. *Aeronaut. Comput. Tech.* **2014**, *44*, 64–67.
13. Zi, B.; Jiang, F.; Wu, Y.; Bai, H.; Tang, Y.; Lu, C. Analysis and experimental research on vibration reduction in ship high-temperature pipeline based on long coated damping structure. *J. Mar. Sci. Eng.* **2021**, *9*, 838. [CrossRef]
14. Jiang, J.; Zhang, P.; Patil, D.; Li, H.N.; Song, G. Experimental studies on the effectiveness and robustness of a pounding tuned mass damper for vibration suppression of a submerged cylindrical pipe. *Struct. Control. Health Monit.* **2017**, *24*, e2027. [CrossRef]
15. Lu, Z.; Lu, X.L.; Masri, S.F. Studies of the performance of particle dampers under dynamic loads. *J. Sound Vib.* **2010**, *329*, 5415–5433. [CrossRef]
16. Shah, B.M.; Pillet, D.; Bai, X.M.; Keer, L.M.; Wang, Q.J.; Snurr, R.Q. Construction and characterization of a particle-based thrust damping system. *J. Sound Vib.* **2009**, *326*, 489–502. [CrossRef]
17. Cui, Z.; Wu, J.H.; Chen, H.; Li, D. A quantitative analysis of the energy dissipation mechanism of the non-obstructive particle damping technology. *J. Sound Vib.* **2011**, *330*, 2449–2456. [CrossRef]
18. Masri, S.F. General motion of impact dampers. *J. Acoust. Soc. Am.* **1970**, *47*, 229–237. [CrossRef]
19. Xu, Z.; Wang, M.Y.; Chen, T. Particle damping for passive vibration suppression: Numerical modelling and experimental investigation. *J. Sound Vib.* **2005**, *279*, 1097–1120. [CrossRef]
20. Jin, G.; Zhao, Z.; Liu, B.; Cun, W.; Zhao, Z.; Hou, M.; Chen, G. Design of a particle damper and experimental study on vibration damping of the pipeline. *Adv. Mech. Eng.* **2021**, *13*, 1–14. [CrossRef]
21. Meyer, N.; Seifried, R. Numerical and experimental investigations in the damping behavior of particle dampers attached to a vibrating structure. *Comput. Struct.* **2020**, *238*, 106281. [CrossRef]

22. Jin, J.; Yang, W.; Koh, H.I.; Park, J. Development of tuned particle impact damper for reduction of transient railway vibrations. *Appl. Acoust.* **2020**, *169*, 107487. [CrossRef]
23. Yang, M.Y. *Development of Master Design Curves for Particle Impact Dampers*; The Pennsylvania State University: State College, PA, USA, 2003.
24. Romdhane, M.B.; Bouhaddi, N.; Trigui, M.; Foltête, E.; Haddar, M. The loss factor experimental characterisation of the non-obstructive particles damping approach. *Mech. Syst. Signal Process.* **2013**, *38*, 585–600. [CrossRef]
25. Wang, J.; Juan, M.; Yang, S.; Zhang, D.; Zhang, Z.; Jin, J.; Yu, T. Experimental investigation of the vibration reduction of the pipeline system with a particle impact damper under harmonic excitation. *Appl. Sci.* **2023**, *13*, 618. [CrossRef]
26. Guo, H.; Ichikawa, K.; Sakai, H.; Zhang, H.; Zhang, X.; Tsuruta, K.; Makihara, K.; Takezawa, A. Numerical and experimental analysis of additively manufactured particle dampers at low frequencies. *Powder Technol.* **2022**, *396*, 696–709. [CrossRef]
27. Żurawski, M.; Zalewski, R. Damping of beam vibrations using tuned particles impact damper. *Appl. Sci.* **2020**, *10*, 6334. [CrossRef]
28. Xu, Z.L. *Elasticity*; Higher Education Press: Beijing, China, 1990.